Journal of Medicinal Chemistry

Article

Synthesis and Evaluation of Novel Radioligands Based on 3-[5-(Pyridin-2-yl)-2*H*-tetrazol-2-yl]benzonitrile for Positron Emission Tomography Imaging of Metabotropic Glutamate Receptor Subtype 5

Yoko Shimoda, Tomoteru Yamasaki, Masayuki Fujinaga, Masanao Ogawa, Yusuke Kurihara, Nobuki Nengaki, Katsushi Kumata, Joji Yui, Akiko Hatori, Lin Xie, Yiding Zhang, Kazunori Kawamura, and Ming-Rong Zhang

J. Med. Chem., **Just Accepted Manuscript** • DOI: 10.1021/acs.jmedchem.6b00209 • Publication Date (Web): 25 Mar 2016

ACS Publications

Journal of Medicinal Chemistry is published by the American Chemical Society. 1155 Sixteenth Street N.W., Washington, DC 20036

Synthesis and Evaluation of Novel Radioligands Based on 3-[5-(Pyridin-2-yl)-*2H*-tetrazol-2-yl]benzonitrile for Positron Emission Tomography Imaging of Metabotropic Glutamate Receptor Subtype 5

*Yoko Shimoda,[†,§] Tomoteru Yamasaki,[†,§] Masayuki Fujinaga,[†,§] Masanao Ogawa,[†,‡] Yusuke Kurihara,[†,‡] Nobuki Nengaki,[†,‡] Katsushi Kumata,[†] Joji Yui,[†] Akiko Hatori,[†] Lin Xie,[†] Yiding Zhang,[†] Kazunori Kawamura,[†] and Ming-Rong Zhang[†,]**

[†]Department of Molecular Probes, Molecular Imaging Center, National Institute of Radiological Sciences, 4-9-1 Anagawa, Inage-ku, Chiba 263-8555, Japan

[‡]SHI Accelerator Service Co. Ltd., 1-17-6 Osaki, Shinagawa-ku, Tokyo 141-0032, Japan

[§]These authors contributed equally.

*Correspondence to:

Ming-Rong Zhang, PhD

Phone: +81-43-382-3709; Fax: +81-43-206-3261; E-mail: zhang@nirs.go.jp

Department of Molecular Probes, Molecular Imaging Center, National Institute of Radiological Sciences, 4-9-1 Anagawa, Inage-ku, Chiba 263-8555, Japan

ABSTRACT

We designed five 3-[5-(pyridin-2-yl)-2*H*-tetrazol-2-yl]benzonitrile analogs as candidates for positron emission tomography (PET) imaging of metabotropic glutamate receptor subtype 5 (mGluR5). Among these compounds, 3-methyl-5-(5-(pyridin-2-yl)-2*H*-tetrazol-2-yl)benzonitrile (**10**) exhibited high binding affinity (K_i = 9.4 nM) and moderate lipophilicity (cLogD: 2.4). Subsequently, [^{11}C]**10** was radiosynthesized at 25 ± 14% radiochemical yield (n = 11) via *C*-[^{11}C]methylation of the arylstannyl precursor **15** with [^{11}C]methyl iodide. In vitro autoradiography and PET assessment using [^{11}C]**10** showed high specific binding in the striatum and hippocampus, two brain regions enriched with mGluR5. Moreover, test-retest PET studies with [^{11}C]**10** indicated high reliability to quantify mGluR5 density, such as the intraclass correlation coefficient (0.90) and Pearson r (0.91) in the striatum of rat brain. We demonstrated that [^{11}C]**10** is a useful PET ligand for imaging and quantitative analysis of mGluR5. Furthermore, [^{11}C]**10** might be modified using its skeleton as a lead compound.

INTRODUCTION

Glutamate is the major excitatory neurotransmitter in the brain and its receptors are classified into two types, ionotropic and metabotropic. Metabotropic glutamate receptors (mGluRs) are G protein-coupled receptors categorized into three groups including eight subtypes (mGluR1–8) based on their structure, signal transduction pathways, and pharmacological properties.[1,2] Of these groups, group I mGluRs (mGluR1 and mGluR5) are localized postsynaptically in glutamatergic neurons, activate phospholipase C after G_q protein coupling, and subsequently form inositol 1,4,5-triphosphate and triacylglycerol. These second messengers promote intracellular calcium release, finally activating protein kinase C.[3,4] Although mGluR1 and mGluR5 have a high degree of homology, each receptor has a distinct regional distribution in the brain.[5,6] The mGluR5 is mainly expressed in the striatum and can trigger the activities of the *N*-methyl-D-aspartate receptor and dopamine transporter, and modulate neurotransmission in the central nervous system (CNS).[7,8] Based on the physiological properties, a number of modulators targeting mGluR5 have been developed for treatment of several CNS disorders such as anxiety, depression, fragile X syndrome, and dyskinesia in Parkinson's disease.[9–11] Subsequently, several positron emission tomography (PET) ligands for mGluR5 imaging were developed with chemical structures based on 2-methyl-6-(phenylethynyl)pyridine (MPEP, **1**)[12] and 3-[(2-methyl-1,3-thiazol-4-yl)ethynyl]pyridine (MTEP, **2**), two positive allosteric mGluR5 modulators.[13] These PET ligands labeled with carbon-11 (^{11}C; half-life: 20.4 min) or fluorine-18 (^{18}F; half-life: 109.8 min) show specific accumulation of radioactivity in the mGluR5-enriched striata of

rodent and primate brains.[14,15] Among them, (*E*)-3-((6-methylpyridin-2-yl)ethynyl)cyclohex-2-enone-*O*-[^{11}C]methyloxime ((*E*)-[^{11}C]ABP688, [^{11}C]**3**), (*E*)-3-(pyridin-2-ylethynyl)cyclohex-2-enone-*O*-(3-(2-[^{18}F]-fluoroethoxy)propyl)oxime ([^{18}F]PSS232, [^{18}F]**4**), 3-[^{18}F]fluoro-5-(pyridin-2-ylethynyl)benzonitrile ([^{18}F]FPEB, [^{18}F]**5**), 3-fluoro-5-((2-([^{18}F]fluoromethyl)thiazol-4-yl)ethynyl)benzonitrile ([^{18}F]SP203, [^{18}F]**6**), and 3-fluoro-5-(3-(5-fluoropyridin-2-yl)-1,2,4-oxadiazol-5-yl)benzo-[^{11}C]nitrile ([^{11}C]AZD9272, [^{11}C]**7**) have progressed to clinical studies (Figure 1).[16–19]

Figure 1

The most widely used PET ligand for mGluR5 imaging is [^{11}C]**3**.[20–22] However, it has been reported that the (*Z*) geometrical isomer is also formed while radiosynthesizing [^{11}C]**3** as an (*E*) isomer,[23,24] and the (*Z*) isomer has much poorer efficacy for mGluR5 imaging than [^{11}C]**3**.[25] Ametamey et al. reported approximately 10% (*Z*) isomer during synthesis of [^{11}C]**3** at their PET center.[23] Additionally, we have previously found that conventional radiosynthesis of [^{11}C]**3** at our laboratory includes 20% (*Z*) isomer,[25] and (*Z*) isomer contamination leads to ambiguous results in test-retest PET studies with [^{11}C]**3**.[26,27] Furthermore, average percentage differences between test and retest PET studies with [^{11}C]**3** to determine the nondisplaceable binding potential (BP_{ND}), a quantitative value for evaluation of binding to mGluR5, have been reported as 28% for humans and 12% for baboons in all regions of interest (ROIs). Similarly, test-retest PET studies with radiolabeled

derivatives of **3** also demonstrate relatively low reliability.[28,29] On the other hand, a previous study demonstrated that mGluR5 modulators containing an alkyne moiety formed glutathione conjugates at their alkyne moiety.[30] This result strongly suggests that the presence of an alkyne moiety may produce individual difference of brain uptake of the ligand via catalysis by glutathione S-transferase. Accordingly, development of novel PET ligands lacking the alkyne moiety is desired for in vivo imaging of mGluR5 in the brain.

In the field of medicinal chemistry, tetrazole is known as a bioisoster for alkyne. 3-[5-(Pyridin-2-yl)-2*H*-tetrazol-2-yl]benzonitrile (**8**) has been reported as a new potent antagonist of mGluR5.[31,32] Different from **3**, **4**, **5**, and **6** containing alkyne moieties, compound **8** contains a tetrazole ring. Despite this change, **8** and its derivatives retain relatively high affinities for mGluR5.[31] Additionally, it was expected that **8** have higher affinity for mGluR5 than a previous non-alkyne type ligand **7**.[32]

In this study, to develop a novel PET ligand for mGluR5 imaging, we designed five ligands, **9**–**13** (Figure 2), using **8** as a lead compound. Compounds **9** and **13** are easily labeled with [^{11}C]methyl iodide ([^{11}C]MeI) or 1-bromo-2-[^{18}F]fluoroethane by [^{11}C]/[^{18}F]alkylation of desmethyl precursor **14**. Compound **10** can be labeled with [^{11}C]MeI by a *C*-[^{11}C] coupling reaction. Since the [^{11}C]CH_3 directly attached to the benzene ring, [^{11}C]**10** may be stable in vivo compared with **9** and **13**. Compounds **11** or **12** bearing fluorine or methyl groups can be labeled with [^{18}F]KF or [^{11}C]MeI at the 6-position in the pyridine ring, which enables investigation of the substituent effect of the

pyridine ring on the in vivo potential. Here, we report the synthesis of PET ligand candidates **9**–**13** as well as in vitro and in vivo evaluations of their potential for imaging mGluR5 in the brain.

Figure 2

RESULTS AND DISCUSSION

Chemistry. It has been found that some 1,3-disubstituted aryl compounds derived from **3** and **8** show similar or improved binding affinities compared with their corresponding parent compounds.[31] Here, we synthesized 1,3-disubstituted analogs **9**–**13** of **8** (Scheme 1). To label **9** and **10**, we synthesized precursors **14** and **15**.

To construct a tetrazole ring, a 1,3-dipolar cycloaddition reaction was performed between tosyl hydrazone **20** and aryldiazonium salt **24**. Compound **20** was synthesized by reacting 2-pyridinecarboxaldehydes **17**–**19** with *p*-toluenesulfonyl hydrazide, which was used for the next reaction without purification. Diazonium compound **24** was prepared by reacting anilines **21**–**23** with $NaNO_2$ under acidic conditions in situ. The reaction of **20** and **24** under basic conditions produced tetrazole compounds **9**–**12** and **16** with 23–50% chemical yields. Demethylation of **9** using BBr_3 was conducted at −40 °C to produce **14** that was used for the subsequent fluoroethylation to yield **13**. Stannylation of **16** using bis(tributyltin) in the presence of $Pd(PPh_3)_4$ did not produce the tributylstannyl compound. In place of bis(tributyltin), reacting **16** with bis(trimethyltin), a more reactive reagent for stannylation, produced the trimethylstannyl compound **15** with a 24% chemical

yield.

Scheme 1

In Vitro Profiles of PET Ligand Candidates. The binding affinities of PET ligand candidates **9**–**13** for mGluR5 were measured using a binding assay with the mGluR5-selective radioligand [^{11}C]**3** in rat brain homogenates. As shown in Figure 3 and Table 1, these compounds exhibited a wide range of binding affinities for mGluR5 with K_i values of 9.4–2280 nM. The K_i values of compounds **9** and **10** in the assay with [^{11}C]**3** were 10.8 and 9.4 nM, respectively. This result was similar to previous data in which the K_i values of **9** and **10** were 6 and 7 nM for mGluR5 in an assay with competition to 3-[^{3}H]methoxy-5-(pyridin-2-ylethynyl)pyridine.[31] The change of the methoxy group in **9** to a relatively large fluoroethoxy group in **13** significantly decreased the binding affinity for mGluR5. These results suggested that the presence of only small substituents, such as methyl and methoxy groups, at the 3-position of the benzene ring provided a better fit for the binding site of the mGluR5 domain, although the affinities of **9** and **10** were slightly weaker than that of **3** (K_i = 5.5 nM). On the other hand, compounds **11** and **12** with a fluorine atom and methyl group at the 6-position of the pyridine ring showed low affinities for mGluR5. This result was different from the high affinities of compounds **1** and **3** for mGluR5, which included 6-methylpyridine moieties, and the reason remains unclear.

The values of calculated (cLogD) and measured lipophilicity (LogD) are shown in Table 1. The

cLogD values for compounds **9**–**13** were 2.4–2.9, which were within the range generally considered to be suitable for PET ligands in brain imaging.[33] Following radiolabeling with ^{11}C, the LogD values were measured for [^{11}C]**9** and [^{11}C]**10** (radiochemical results are described in the following section). The LogD values of [^{11}C]**9** and [^{11}C]**10** were 2.4 and 2.8, which were similar and higher than that of [^{11}C]**3** (LogD = 2.4), respectively.

Figure 3

Table 1

Radiochemistry. Because of their potent binding affinities for mGluR5, we selected compounds **9** and **10** for radiolabeling with [^{11}C]MeI. [^{11}C]MeI was produced by reducing cyclotron-produced [^{11}C]CO_2 with $LiAlH_4$, followed by iodination with 57% HI (Scheme 2). To yield [^{11}C]**9**, *O*-[^{11}C]methylation of desmethyl precursor **14** with [^{11}C]MeI in the presence of NaOH proceeded easily at 70 °C for 5 min. For [^{11}C]**10**, arylstannyl precursor **15** was added to a mixture containing [^{11}C]MeI and a Pd catalyst, which was prepared in a reaction vial containing $Pd_2(dba)_3$, CuCl, and P(*o*-tol)$_3$ in DMF. This reaction mixture was heated at 80 °C for 5 min. After termination of the *O*- and *C*-[^{11}C]methylation reactions, separation of these mixtures was performed by reverse phase HPLC to obtain two formulated products, [^{11}C]**9** and [^{11}C]**10**, respectively.

Starting from 14.8–22.2 GBq [^{11}C]CO_2, 0.58–0.91 GBq [^{11}C]**9** was produced with 14 ± 4% (*n* = 3) radiochemical yield at 32 min after the end of bombardment (EOB). Starting from 22.2–28.1 GBq

[^{11}C]CO_2, 0.86–2.99 GBq [^{11}C]**10** was obtained with 25 ± 14% (n = 11) radiochemical yield at 32 min after EOB. In the final product solution, the specific activities of [^{11}C]**9** and [^{11}C]**10** were 57–71 and 52–190 GBq/μmol, respectively. The radiochemical purity of both products was higher than 98% at the end of synthesis (EOS).

The two products did not show radiolysis at room temperature for 90 min after formulation, indicating their radiochemical stability for the duration of at least one PET scan. The analytical results of [^{11}C]**9** and [^{11}C]**10** were in compliance with our in-house quality control/assurance specifications for radiopharmaceuticals.

Scheme 2

In Vitro Autoradiography. To confirm the specificity and selectivity of [^{11}C]**9** and [^{11}C]**10** binding to mGluR5, in vitro autoradiography was performed using rat brain sections (Figure 4). In the control sections for both radioligands (A and D), the distribution pattern of radioactivity was heterogeneous with the highest level in the striatum. Moderate radioactivity was seen in the hippocampus and cerebral cortex, and a low level was found in the thalamus. The lowest radioactivity was seen in the cerebellum. This distribution pattern was consistent with the biological distribution of mGluR5 in the rat brain.[34] Co-incubation with mGluR5-selective compound **1** (1 μM) dramatically diminished the radioactivity in the brain sections of both groups (B and E). Furthermore, co-incubation with mGluR1-selective (3,4-dihydro-2H-pyrano[2,3]b quinolin-7-yl) (cis-4-methoxycyclohexyl)

methanone (JNJ16259685, **25**)[35] (1 μM) had almost no effect on the binding of [^{11}C]**9** and [^{11}C]**10** (C and F).

Figure 4

Table 2 shows the ratios of radioactive binding in interesting regions to the cerebellum, a region of negligible mGluR5 expression, as determined from autoradiograms of [^{11}C]**9** and [^{11}C]**10**. In the control sections, the ratios of the mGluR5-richest striatum to cerebellum were 14.9 for [^{11}C]**9** and 15.8 for [^{11}C]**10**. By co-incubation with compound **1**, these ratios decreased to 2.7 for [^{11}C]**9** and 2.1 for [^{11}C]**10**. These results indicated that [^{11}C]**10** had higher specific binding for mGluR5 and lower nonspecific binding than [^{11}C]**9**.

Table 2

Because of the high level of in vitro-specific binding to mGluR5 in the rat brain, we pursed [^{11}C]**10** for in vivo evaluation using PET to assess its potential for mGluR5 imaging in the brain.

PET Assessment. To evaluate the in vivo availability of [^{11}C]**10**, PET assessments were performed using rats.

Figure 5 shows time-activity curves (TACs) of [^{11}C]**10** in the striatum, hippocampus, frontal cortex, thalamus, and cerebellum of the baseline (A)- and compound **1** (1 mg/kg) (B)-treated rats. In baseline rats (n = 7), radioactivities in all ROIs immediately reached maximum levels after injection

of [^{11}C]**10** and then decreased quickly. The uptake ratio [$C_{tissue}(t)/C_{cerebellum}(t)$] of each region in the cerebellum at the equilibrium state [$C_{tissue}(t)dt/C_{cerebellum}(t)dt = 0$] of specific binding was 3.0 ± 0.1 in the striatum, 2.4 ± 0.1 in the hippocampus, 2.3 ± 0.1 in the frontal cortex, and 2.0 ± 0.1 in the thalamus (Supporting Information Figure 4A). In blocking experiments (n = 4), the ratios were reduced by 1.3–1.6 in each brain region (Supporting Information Figure 4B). These results suggested that [^{11}C]**10** showed significant specific binding to mGluR5. The BP_{ND} value of [^{11}C]**10** was estimated by kinetic analysis with the simplified reference tissue model (SRTM)[36] to quantitatively evaluate the binding to target molecules in vivo.[37] The BP_{ND} of [^{11}C]**10** in each region was 1.30 ± 0.10 in the striatum, 0.94 ± 0.09 in the hippocampus, 0.82 ± 0.09 in the frontal cortex, and 0.72 ± 0.09 in the thalamus. As shown in Figure 6, parametric PET images of [^{11}C]**10** with the BP_{ND} scale clearly visualized regional differences with the highest signal in the striatum. Moderate signals were detected in the hippocampus and cerebral cortex. Low radioactivity was found in the pons and cerebellum. These specific signals were homogenously diminished by pretreatment with **1** (1 mg/kg), demonstrating that PET using [^{11}C]**10** provided significant specific visualization of mGluR5 in brain regions.

Figure 5

Figure 6

Table 3 shows the reliability of test-retest PET studies with [^{11}C]**10**. A scatter plot comparing the

individual outcomes is shown in Figure 7. In the striatum, which is the mGluR5-richest region in the brain, the percentage of variability, intraclass correlation coefficient (ICC), and Pearson's correlation coefficient (*r*) were 3.0, 0.90, and 0.91, respectively. Additionally, correlation (Pearson's *r*) between test and retest outcomes in all ROIs was 0.96, indicating high reliability of PET with [^{11}C]**10**.

Table 3

Figure 7

Ex Vivo Metabolite Analysis. To investigate metabolism of [^{11}C]**10** in the plasma and brain, metabolite analysis was performed using rats (Figure 8). The fraction corresponding to unchanged [^{11}C]**10** (t_R = 5.2–5.6 min) in the plasma gradually decreased to 57 ± 19% at 5 min, 18 ± 4% at 30 min, and 11 ± 3% at 60 min after injection. A polar radiolabeled metabolite (t_R = 2.1–2.4 min) was observed in the HPLC charts of plasma and brain samples (Supporting Information Figure 5). On the other hand, unchanged [^{11}C]**10** in the brain remained at 93% of total radioactivity at 30 min and decreased to 84% at 60 min. Considering that the treated brain homogenate was slightly contaminated with blood from sampling and brain capillaries (3−5% of whole rat brain[38]) the actual percentages of unchanged [^{11}C]**10** in the brain tissue might be larger than the experimentally determined values. Because the radioactive uptake of [^{11}C]**10** in the brain was very low from 30 min after injection, metabolite correction for quantitative analysis was unnecessary.

Figure 8

Comparison of [^{11}C]3 and [^{11}C]10. To confirm the utility of [^{11}C]**10** for PET, we compared [^{11}C]**10** with [^{11}C]**3**, the most widely used PET ligand for mGluR5 imaging.

The in vitro binding affinities of both unlabeled compounds for mGluR5 were measured under the same experimental conditions. Although the binding affinity of compound **10** (K_i = 9.4 nM) for mGluR5 was slightly weaker than that of **3** (K_i = 5.5 nM), [^{11}C]**10** showed significant in vitro-specific binding on the autoradiograms of rat brain sections (Figure 4).

The average BP_{ND} value of [^{11}C]**10** in PET assessments using Sprague-Dawley (SD) rats was half of that of [^{11}C]**3**: 1.30 vs. 2.49 ([^{11}C]**10** vs. [^{11}C]**3**) in the striatal BP_{ND}.[39] However, as an important index in quantitative PET analysis, the test-retest reliability of SRTM analysis with [^{11}C]**10** in the striatum of the rat brain was superior to that with [^{11}C]**3**: 3.0 vs. 4.8 ([^{11}C]**10** vs. [^{11}C]**3**) for the percentage of variability; 0.90 vs. 0.88 for ICC, and 0.91 vs. 0.88 for Pearson's *r*. Moreover, the in vivo stability of [^{11}C]**10** in rat plasma was higher than that of [^{11}C]**3**. At 5 min after injection, the percentage of unchanged radioligand was 57% for [^{11}C]**10** and <40% for [^{11}C]**3**,[40] which might be caused by different metabolizing routes of the radioligands.

Taken together, although the in vitro- and in vivo-binding affinities of [^{11}C]**10** for mGluR5 were slightly weaker than those of [^{11}C]**3**, the high test-retest reliability of PET and in vivo stability of [^{11}C]**10** provide some advantages, especially in improving incoherence, which has been found in quantitative PET analysis with [^{11}C]**3** for mGluR5 imaging in animal and human studies.[26–29]

Biodistribution Analysis. The distribution of radioactivity in mice was measured at five time points (1, 5, 15, 30, and 60 min) after injection of [^{11}C]**10** (Figure 9). At 1 min, high uptake (>5% injected dose per gram of wet tissue, %ID/g) appeared in the lung (6.3 ± 0.8), liver (7.0 ± 1.6), kidney (6.0 ± 0.6), small intestines (7.0 ± 2.5), and brain (5.2 ± 0.6 %ID/g). After the initial increments, the radioactivity in many tissues decreased dramatically, while that in the liver and small intestines increased continually until reaching maximum levels (liver: 13.6 ± 1.0 %ID/g at 5 min; small intestines: 47.7 ± 14.1 %ID/g at 15 min) and then decreased quickly. Accumulation of radioactivity in the liver and small intestines suggested that hepatobiliary excretion as well as the intestinal reuptake pathway might dominate the whole body distribution of radioactivity and rapid washout from the body after injection.

Figure 9

SUMMARY

In the current study, we demonstrated that compound **10** is a promising PET ligand candidate for mGluR5 imaging by in vitro binding assays, and subsequently synthesized [^{11}C]**10** via *C*-[^{11}C]methylation of the trimethylstannyl precursor **15** with [^{11}C]MeI in a short synthesis time with reliable radiochemical yield. PET with [^{11}C]**10** in rat brains visualized the regional distribution of

mGluR5 and demonstrated high reliability for quantification of the mGluR5 density in test-retest PET studies. Hence, [^{11}C]**10** is a potential PET ligand for imaging and quantification of mGluR5 in the brain, which may warrant evaluation in humans. This radioligand is also a useful lead compound for development of new PET ligands with higher affinity and more specific binding to mGluR5.

EXPERIMENTAL SECTION

Melting points were measured using a micro melting point apparatus (MP-500P, Yanaco, Tokyo, Japan) and were uncorrected. ^{1}H NMR (300 MHz) and ^{13}C NMR (75 MHz) spectra were recorded on a JEOL-AL-300 spectrometer (JEOL, Tokyo, Japan) using TMS as an internal standard. All chemical shifts (δ) are reported as ppm downfield relative to the TMS signal. Signals are quoted as s (singlet), d (doublet), t (triplet), br (broad), or m (multiplet). FAB-MS and HRMS spectra were obtained on a NMS-SX102 spectrometer (JEOL) and recorded on the spectrometer. Silica gel column chromatography was performed using Wako gel C-200 (70–230 mesh, Wako Pure Chemical Industries, Osaka, Japan). HPLC analysis was performed using the JASCO HPLC system (JASCO, Tokyo, Japan) and a Capcell Pak C_{18} column (4.6 mm i.d. × 250 mm, Shiseido, Tokyo). Compounds **9**–**15** indicated ≥ 95% purity by HPLC analysis. The chemical purities of compounds **9**–**15** were analyzed under the following conditions: **9**, **13**, and **14**: 1.0 mL/min, MeCN/H_2O/Et_3N (50/50/0.1, v/v/v); **10** and **15**: 1.5 mL/min, MeCN/H_2O/Et_3N (55/45/0.1, v/v/v); **11** and **12**: 1.0 mL/min, MeCN/H_2O/Et_3N (60/40/0.1, v/v/v). Radiochemical purity of [^{11}C]**9** and [^{11}C]**10** was analyzed by

HPLC with a detector to monitor radioactivity under the following conditions: [^{11}C]**9**: 1.0 mL/min, MeCN/H_2O/Et_3N (50/50/0.1, v/v/v); [^{11}C]**10**: 1.5 mL/min, MeCN/H_2O/Et_3N (55/45/0.1, v/v/v). For radio-HPLC separation and analysis, effluent radioactivity was monitored using a NaI (Tl) scintillation detector system. All chemical reagents and solvents were purchased from commercial sources (Sigma-Aldrich, St. Louis, MO; Wako Pure Chemical Industries; Tokyo Chemical Industries, Tokyo, Japan) and used as supplied. Compounds **1** hydrochloride and **25** were purchased from Enzo Life Sciences (Farmingdale, NY).

[^{11}C]CO_2 was produced by a CYPRIS HM18 cyclotron (Sumitomo Heavy Industry, Tokyo, Japan). [^{11}C]MeI was synthesized from cyclotron-produced [^{11}C]CO_2 as described previously.[41]

[^{11}C]**3** for the in vitro binding assay was synthesized according to a previous report.[25] At EOS (n = 3), 2.3–3.5 GBq [^{11}C]**3** was obtained with >99% radiochemical purity and 113–239 GBq/μmol SA.

Chemistry

3-Methoxy-5-(5-(pyridin-2-yl)-2H-tetrazol-2-yl)benzonitrile (9). A mixture of 3-amino-5-methoxybenzonitrile (296 mg, 2 mmol), ethanol (6 mL), and 42% aqueous tetrafluoroboric acid (1.4 mL) was stirred at −5 °C in an ice-salt bath. A solution of $NaNO_2$ (152 mg, 2.2 mmol) in water (1 mL) was added dropwise to this mixture to produce a solution of diazonium salt. In another flask, a mixture of 2-pyridinecarboxaldehyde (214 mg, 2 mmol) and *p*-toluenesulfonyl hydrazide (372 mg, 2 mmol) in ethanol (5 mL) was stirred at room temperature for

15 min. Following removal of ethanol under reduced pressure, the residue was dissolved in pyridine (2 mL) and cooled to −10 °C. The solution of diazonium salt was added dropwise to this mixture, followed by stirring at room temperature for 3.5 h. The reaction mixture was poured into water and extracted with CH_2Cl_2. The organic layer was washed with brine, dried over anhydrous Na_2SO_4, and concentrated under reduced pressure. Purification of the residue by silica gel column chromatography (ethyl acetate/*n*-hexane, 1/2 to 1/1, v/v) yielded **9** (269 mg, 48%) as slightly orange crystals (mp: 176–177 °C). ^{1}H NMR ($CDCl_3$): δ 3.98 (3H, s), 7.30 (1H, s), 7.46–7.50 (1H, m), 7.91–7.96 (1H, m), 8.06 (1H, dd, *J* = 1.8, 1.8 Hz), 8.20 (1H, s), 8.37 (1H, d, *J* = 8.0 Hz), 8.86 (1H, d, *J* = 4.8 Hz). ^{13}C NMR ($CDCl_3$): δ 56.3, 109.8, 114.7, 115.4, 117.2, 119.1, 123.0, 125.4, 137.3, 138.1, 146.0, 150.6, 160.8, 165.2. HRMS *m/z*: 279.1046 (calculated for $C_{14}H_{11}N_6O$: 279.0994).

3-Methyl-5-(5-(pyridin-2-yl)-2H-tetrazol-2-yl)benzonitrile (10). A mixture of 3-amino-5-methylbenzonitrile (90 mg, 0.7 mmol), ethanol (2 mL), and 42% aqueous tetrafluoroboric acid (555 μL) was stirred at −5 °C in an ice-salt bath. A solution of $NaNO_2$ (52 mg, 0.8 mmol) in water (1 mL) was added dropwise to this mixture to produce a solution of diazonium salt. In another flask, a mixture of 2-pyridinecarboxaldehyde (65 μL, 0.7 mmol) and *p*-toluenesulfonyl hydrazide (128 mg, 0.7 mmol) in ethanol (2 mL) was stirred at room temperature for 20 min. After removal of ethanol under reduced pressure, the residue was dissolved in pyridine (2.0 mL) and cooled to −5 °C. The solution of diazonium salt was added dropwise to this solution, followed by stirring at room

temperature for 2 h. The reaction mixture was poured into water and extracted with CH_2Cl_2. The organic layer was washed with brine, dried over anhydrous Na_2SO_4, and concentrated under reduced pressure. Purification of the residue by silica gel column chromatography (CH_2Cl_2 to ethyl acetate/CH_2Cl_2, 1/9, v/v) yielded **10** (86 mg, 48%) as slightly orange crystals (mp: 139 °C). ^{1}H NMR ($CDCl_3$): δ 2.55 (3H, s), 7.45–7.50 (1H, m), 7.62 (1H, s), 7.90–7.96 (1H, m), 8.34–8.41 (3H, m), 8.84–8.86 (1H, m). ^{13}C NMR ($CDCl_3$): δ 21.2, 100.5, 113.9, 117.4, 120.5, 123.0, 124.6, 125.4, 133.6, 136.9, 137.3, 141.8, 146.1, 150.6. HRMS *m/z*: 263.0988 (calculated for $C_{14}H_{11}N_6$: 263.1045).

3-(5-(6-Fluoropyridin-2-yl)-2H-tetrazol-2-yl)-5-methoxybenzonitrile (11). A mixture of 3-amino-5-methoxybenzonitrile (148 mg, 1 mmol), ethanol/water (4 mL, 1/1, v/v), and conc. HCl (250 μL) was stirred at −5 °C in an ice-salt bath. A solution of $NaNO_2$ (76 mg, 1.1 mmol) in water (1 mL) was added dropwise to this mixture to produce a solution of diazonium salt. In another flask, a mixture of 6-fluoropyridine-2-carboxaldehyde (182 mg, 1.4 mmol) and *p*-toluenesulfonyl hydrazide (182 mg, 1.0 mmol) in ethanol (5.0 mL) was stirred at room temperature for 1 h, followed by addition of 1 M NaOH (5.0 mL). After the solution was cooled to −10 °C, the solution of diazonium salt was added dropwise, followed by stirring at room temperature for 2 h. This reaction mixture was poured into water and extracted with ethyl acetate. The organic layer was washed with brine, dried over anhydrous Na_2SO_4, and concentrated under reduced pressure. Purification of the residue by silica gel column chromatography (CH_2Cl_2 to ethyl acetate/CH_2Cl_2, 1/9, v/v) yielded **11** (67 mg,

23%) as slightly yellow crystals (mp: 172–174 °C). ^{1}H NMR ($CDCl_3$): δ 3.98 (3H, s), 7.14 (1H, dd, *J* = 2.9, 8.0 Hz), 7.30–7.32 (1H, m), 8.03–8.08 (2H, m), 8.18 (1H, dd, *J* = 1.5, 1.5 Hz), 8.21 (1H, dd, *J* = 2.2, 7.5 Hz). ^{13}C NMR ($CDCl_3$): δ 56.4, 109.8, 111.8 (d, $J_{C\text{-}F}$ = 36.4 Hz), 114.8, 115.4, 117.1, 119.2, 120.4 (d, $J_{C\text{-}F}$ = 3.2 Hz), 138.0, 142.4 (d, $J_{C\text{-}F}$ = 7.4 Hz), 144.4 (d, $J_{C\text{-}F}$ = 14.2 Hz), 160.8, 164.0, 163.6 (d, $J_{C\text{-}F}$ = 241.1 Hz). HRMS *m/z*: 297.0896 (calculated for $C_{14}H_{10}ON_6F$: 297.0900).

3-Methoxy-5-(5-(6-methylpyridin-2-yl)-2H-tetrazol-2-yl)benzonitrile (12). A mixture of 3-amino-5-methoxybenzonitrile (297 mg, 2 mmol), ethanol (6 mL), and 42% aqueous tetrafluoroboric acid (1.4 mL) was stirred at −5 °C in an ice-salt bath. A solution of $NaNO_2$ (158 mg, 2.3 mmol) in water (1 mL) was added dropwise to produce a solution of diazonium salt. In another flask, a mixture of 6-methyl-2-pyridinecarboxaldehyde (250 mg, 2.1 mmol) and *p*-toluenesulfonyl hydrazide (382 mg, 2.1 mmol) in ethanol (6.0 mL) was stirred at room temperature for 15 min. After removal of ethanol under reduced pressure, the residue was dissolved in pyridine (2.0 mL). After the solution was cooled to −10 °C, the solution of diazonium salt was added dropwise, followed by stirring at room temperature for 3.5 h. The reaction mixture was poured into CH_2Cl_2, washed with brine, dried over anhydrous Na_2SO_4, and concentrated under reduced pressure. Purification of the residue by silica gel column chromatography (CH_2Cl_2) and then recrystallization from CH_2Cl_2/*n*-hexane yielded **12** (296 mg, 50%) as colorless crystals (mp, 178–180 °C). ^{1}H NMR ($CDCl_3$): δ 2.73 (3H, s), 3.98 (3H, s), 7.29 (1H, dd, *J* = 1.5, 2.6 Hz), 7.34 (1H, d, *J* = 7.7 Hz), 7.81

(1H, dd, J = 7.7, 7.7 Hz), 8.05 (1H, dd, J = 2.2, 2.2 Hz), 8.13 (1H, s), 8.16 (1H, dd, J = 1.5, 1.5 Hz). ^{13}C NMR ($CDCl_3$): δ 24.6, 56.3, 109.8, 114.5, 115.3, 117.2, 119.0, 120.2, 125.2, 137.4, 138.0, 145.3, 159.6, 160.7, 165.3. HRMS *m/z*: 293.1108 (calculated for $C_{15}H_{13}N_6O$: 293.1151).

3-(2-Fluoroethoxy)-5-(5-(pyridin-2-yl)-2H-tetrazol-2-yl)benzonitrile (13). A mixture of **14** (100 mg, 0.4 mmol), K_2CO_3 (78 mg, 0.6 mmol), and 2-fluoroethyl-4-methylbenzenesulfonate (92 mg, 0.4 mmol) in DMF (3 mL) was stirred at 70 °C for 5 h. The reaction mixture was poured into saturated aqueous K_2CO_3 and extracted with CH_2Cl_2. The organic layer was dried over anhydrous Na_2SO_4 and concentrated under reduced pressure. Purification of the residue by silica gel column chromatography (ethyl acetate/*n*-hexane, 2/3, v/v) yielded **13** (40 mg, 34%) as colorless crystals (mp: 171–173 °C). ^{1}H NMR ($CDCl_3$): δ 4.39 (2H, dt, J = 4.0, 27.4 Hz), 4.82 (2H, dt, J = 4.0, 50.9 Hz), 7.34 (1H, s), 7.48 (1H, dd, J = 1.8, 7.7 Hz), 7.94 (1H, ddd, J = 1.8, 7.7, 7.7 Hz), 8.10 (1H, dd, J = 1.8, 1.8 Hz), 8.23 (1H, s), 8.36 (1H, d, J = 7.7 Hz), 8.86 (1H, d, J = 4.4 Hz). ^{13}C NMR ($CDCl_3$): δ 68.3 (d, $J_{C\text{-}F}$ = 20.3 Hz), 81.2 (d, $J_{C\text{-}F}$ = 171.4 Hz), 110.2, 114.9, 115.9, 117.0, 119.8, 123.1, 125.4, 137.3, 138.1, 146.0, 150.6, 159.7, 165.3. HRMS *m/z*: 311.1089 (calculated for $C_{15}H_{12}FN_6O$: 311.1057).

3-Hydroxy-5-(5-(pyridin-2-yl)-2H-tetrazol-2-yl)benzonitrile (14). BBr_3 (1 M) in CH_2Cl_2 (5 mL) was added dropwise to a solution of **9** (278 mg, 1 mmol) in CH_2Cl_2 (20 mL) at −40 °C. The reaction mixture was warmed to room temperature slowly and stirred overnight. Then, the reaction mixture

was adjusted to pH 7 with saturated aqueous Na_2CO_3 and extracted with ethyl acetate. The organic layer was washed with brine, dried over anhydrous Na_2SO_4, and concentrated under reduced pressure. Purification of the residue by silica gel column chromatography (ethyl acetate/*n*-hexane, 1/1, v/v) yielded **14** (251 mg, 95%) as slightly orange crystals (mp: 211–212 °C). ^{1}H NMR (DMSO-d_6): δ 7.42 (1H, s), 7.60–7.65 (1H, m), 7.87 (1H, s), 8.03–8.10 (2H, m), 8.27 (1H, d, J = 7.7 Hz), 8.80–8.82 (1H, m), 11.2 (1H, br s). ^{13}C NMR (DMSO-d_6): δ 111.5, 113.8, 117.5, 120.5, 122.9, 125.8, 137.6, 137.8, 145.5, 150.4, 159.1, 164.5. HRMS *m/z*: 265.0833 (calculated for $C_{13}H_9N_6O$: 265.0838).

3-(5-(Pyridin-2-yl)-2H-tetrazol-2-yl)-5-(trimethylstannyl)benzonitrile (15). A mixture of **16** (197 mg, 0.6 mmol), hexamethylditin (237 mg, 0.7 mmol), and $Pd(PPh_3)_4$ (36 mg, 5 mol%) in 1,4-dioxane (5 mL) was stirred at 110 °C for 16 h under N_2 gas. The reaction mixture was poured into water and extracted with CH_2Cl_2. The organic layer was washed with brine, dried over anhydrous Na_2SO_4 and concentrated under reduced pressure. Purification of the residue by silica gel column chromatography (ethyl acetate/*n*-hexane, 1/2, v/v) yielded **15** (60 mg, 24%) as colorless crystals (mp: 156–157 °C). ^{1}H NMR ($CDCl_3$): δ 0.44 (9H, s), 7.45–7.50 (1H, m), 7.88–7.96 (2H, m), 8.38 (1H, d, J = 7.7 Hz), 8.50–8.52 (1H, m), 8.60–8.61 (1H, m), 8.85–8.88 (1H, m). ^{13}C NMR ($CDCl_3$): δ −9.03, 113.5, 117.7, 123.0, 125.3, 130.5, 136.2, 137.3, 140.1, 146.2, 147.8, 150.6, 165.2. HRMS *m/z*: 413.0587 (calculated for $C_{16}H_{17}N_6Sn$: 413.0539).

3-Bromo-5-(5-(pyridin-2-yl)-2H-tetrazol-2-yl)benzonitrile (16). A mixture of 3-amino-5-bromobenzonitrile (591 mg, 3.0 mmol), ethanol (4.0 mL), and 42% aqueous tetrafluoroboric acid (2.4 mL) was stirred at −5 °C in an ice-salt bath. A solution of $NaNO_2$ (380 mg, 5.5 mmol) in water (2 mL) was added dropwise to this mixture to produce a solution of diazonium salt. In another flask, a mixture of 2-pyridinecarboxaldehyde (284 μL, 3 mmol) and *p*-toluenesulfonyl hydrazide (563 mg, 3 mmol) in CH_2Cl_2 (4 mL) was stirred at room temperature for 15 min. After removal of CH_2Cl_2 under reduced pressure, the residue was dissolved in pyridine (4 mL). The solution of diazonium salt was added dropwise to this solution at −5 °C, followed by stirring at room temperature for 3.5 h. The reaction mixture was poured into water and extracted with ethyl acetate. The organic layer was washed with brine, dried over anhydrous Na_2SO_4, and concentrated under reduced pressure. Purification of the residue by silica gel column chromatography (ethyl acetate/CH_2Cl_2, 1/9, v/v) yielded **16** (464 mg, 47%) as colorless crystals(mp: 164–166 °C). ^{1}H NMR ($CDCl_3$): δ 7.47–7.52 (1H, m), 7.92–7.97 (2H, m), 8.37 (1H, ddd, *J* = 1.1, 1.1, 8.0 Hz), 8.57 (1H, dd, *J* = 1.8, 1.8 Hz), 8.76 (1H, dd, *J* = 1.8, 1.8 Hz), 8.85–8.88 (1H, m). ^{13}C NMR ($CDCl_3$): δ 115.6, 115.8, 121.8, 123.1, 124.2, 125.6, 127.0, 135.6, 137.3, 137.6, 145.8, 150.6, 165.5. HRMS *m/z*: 326.9983 (calculated for $C_{13}H_8N_6Br$: 326.9994).

Radiochemistry

3-[^{11}C]Methoxy-5-(5-(pyridin-2-yl)-2H-tetrazol-2-yl)benzonitrile ([^{11}C]9). After irradiation, the

cyclotron-produced [^{11}C]CO_2 was bubbled into 0.4 M $LiAlH_4$ in anhydrous THF (0.3 mL). After evaporation of THF, the remaining complex was treated with 57% HI (0.3 mL) to produce [^{11}C]MeI that was distilled and transferred under N_2 gas flow into a solution of **14** (1.3 mg, 4.9 μmol) and NaOH (0.5 M, 7 μL) in anhydrous DMF (0.3 mL) at −15 to −20 °C. When the radioactivity reached a plateau, the reaction mixture was heated at 70 °C for 5 min. The [^{11}C]methylation was competed by addition of MeCN/H_2O/Et_3N (50/50/0.1, 1 mL), and the reaction mixture was applied to a semi-preparative HPLC system. HPLC separation was performed on a Capcell Pak C_{18} column (10 mm i.d. × 250 mm) using MeCN/H_2O/Et_3N (50/50/0.1, v/v/v) at 5 mL/min. The radioactive fraction corresponding to [^{11}C]**9** (t_R = 9.5 min) was collected in a sterile flask, evaporated to dryness under reduced pressure, redissolved in 3 mL sterile saline, and passed through a 0.22-μm Millipore filter to obtain 0.8 GBq [^{11}C]**9**. The identity of [^{11}C]**9** (t_R = 8.6 min) was confirmed by analytical HPLC with unlabeled **9**. The specific activity was calculated by comparing the assayed radioactivity to the mass measured at UV 254 nm.

3-[^{11}C]Methyl-5-(5-(pyridin-2-yl)-2H-tetrazol-2-yl)benzonitrile ([^{11}C]10). Copper(I) chloride (1.5 mg, 15 μmol), CsF (2.8 mg, 19 μmol), and $Pd_2(dba)_3$ (1.4 mg, 1.6 μmol) were added to a 1-mL minivial containing a septum and stirring bar. The vial was purged with nitrogen gas, and a solution of P(*o*-tol)$_3$ (1.8 mg, 5.9 μmol) in DMF (0.2 mL) was added. This mixture was purged with N_2 gas and stirred for 3 min at room temperature. The prepared solution was transferred into a reaction vial

using a syringe equipped with an automated synthetic unit. [^{11}C]MeI was transferred under N_2 gas flow into the reaction vial at −15 to −20 °C. When the radioactivity of [^{11}C]MeI reached a plateau, a solution of precursor **15** in DMF (0.2 mL) was added, and the reaction mixture was heated at 80 °C for 5 min. After 1 mL of the preparative HPLC mobile phase was added, the reaction mixture was filtered through a glass fiber prefilter (GF53, 30 μm; Agilent Technologies, Santa Clara, CA) and applied to the HPLC system. HPLC separation was performed using a Capcell Pak C_{18} column (10 mm i.d. × 250 mm) and MeCN/H_2O/Et_3N (55/45/0.1, v/v/v) at 5.0 mL/min. The radioactive fraction corresponding to [^{11}C]**10** (t_R = 7.7 min) was collected in a sterile flask, evaporated to dryness in vacuo, redissolved in 3 mL sterile normal saline, and passed through a 0.22-μm Millipore filter to yield 2.1 GBq [^{11}C]**10**. The identity of [^{11}C]**10** (t_R = 4.6 min) was confirmed by analytical HPLC with unlabeled **10**. The specific activity was calculated by comparing the assayed radioactivity to the mass measured at UV 254 nm.

Evaluation of Calculated and Measured Lipophilicities. Measurement of the lipophilicities (LogD) of [^{11}C]**9** and [^{11}C]**10** was performed by mixing with *n*-octanol (3 g) and phosphate-buffered saline (PBS; 3 g, 0.1 M, pH 7.4) in a test tube. The tube was vortexed for 3 min at room temperature, followed by centrifugation at 3,500 *g* for 5 min. Aliquots of 0.65 mL PBS and 0.65 mL *n*-octanol were sampled, weighed, and counted. The LogD value was calculated by comparing the ratio of cpm/g of *n*-octanol to that of PBS and expressed as LogD = Log[cpm/g (*n*-octanol)/cpm/g (PBS)].

All measurements were performed in triplicate. The calculated lipophilicities (cLogD) for each ligand were estimated by simulations using ADMET Predictor™ (Simulations Plus, Lancaster, CA).

Animals. The ddY mice (male, 8 weeks old) and SD rats (male, 8–9 weeks old) were purchased from Japan SLC (Shizuoka, Japan), maintained in a temperature-controlled environment with a 12 h light-dark cycle, and fed a standard diet (MB-1; Funabashi Farm, Chiba, Japan).

Ethics Statement. Animals were treated and handled according to the Recommendations for Handling of Laboratory Animals for Biomedical Research compiled by the Committee on the Safety and Ethical Handling Regulations for Laboratory Animal Experiments, National Institute of Radiological Sciences, and this study was approved by the committee.

In Vitro Binding Assay

Three rats were sacrificed by decapitation under anesthesia (3% isoflurane in air). The whole brains except the cerebellum were rapidly removed and homogenized in five volumes of 50 mM Tris-HCl (pH 7.4) containing 120 mM NaCl with a Silent Crusher S homogenizer (Heidolph Instruments, Schwabach, Germany). The homogenate was centrifuged in a polypropylene tube at 40,000 *g* for 15 min at 4 °C using an Optima-TLX (Beckman Coulter, Brea, CA). After discarding the supernatant,

the pellet was resuspended, homogenized, and centrifuged in the same buffer. This procedure was repeated twice to obtain the final pellet of brain homogenate, which was stored at −80 °C before use.

The brain homogenate was diluted to 100 mg/mL in 50 mM Tris-HCl buffer containing 120 mM NaCl, 2 mM KCl, 1 mM $MgCl_2$, and 1 mM $CaCl_2$. Each preparation of 0.1 mL homogenate was incubated with [^{11}C]**3** (1 nM in buffer) and 0.1 mL test compounds **9**–**13** (10^{-2} to 10^{-7} M in 0.1–1% DMSO) in a final volume of 1 mL buffer. These mixtures were incubated for 30 min at room temperature. The bound and free radioactivities were separated by vacuum filtration through 0.3% polyethylenimine-pretreated Whatman GF/C glass fiber filters using a cell harvester (M-24, Brandel, Gaithersburg, MD), followed by three washes with prechilled buffer. The radioactivity of filters containing the bound [^{11}C]**3** was counted with a 1480 Wizard autogamma scintillation counter (Perkin-Elmer, Waltham, MA). In the present study, the radioligand affinity ($1/K_d$) of [^{11}C]**3** for mGluR5 in the brain homogenate was determined using GraphPad Prism 5 (GraphPad Software, La Jolla, CA). The results of inhibitory experiments were subjected to nonlinear regression analysis using GraphPad Prism 5, in which IC_{50} and inhibition constant (K_i) values were calculated.

In Vitro Autoradiography. Rats (n = 3) were killed by cervical dislocation under anesthesia (3% isoflurane in air). Their brains were quickly removed and frozen in crushed dry ice. Sagittal brain sections (20 μm) were prepared with a cryostat (HM560; Carl Zeiss, Oberkochen, Germany). Rat brain sections were preincubated for 10 min in 50 mM Tris-HCl buffer (pH 7.4) containing 1.2 mM

$MgCl_2$ and 2 mM $CaCl_2$ at room temperature. After preincubation, the sections were incubated for 30 min at room temperature in fresh buffer containing [^{11}C]**9** (7.6 MBq, 0.1 nM). For blocking experiments, compounds **1** (1 μM) and **25** (1 μM) were used to determine the specificity and selectivity for mGluR5. After incubation, brain sections were washed (3 × 5 min) with cold buffer, immersed in cold distilled water, and then dried with cold air. The sections were placed in contact with imaging plates (BAS-MS2025, FUJIFILM, Tokyo, Japan). Autoradiograms were obtained and photo-stimulated luminescence (PSL) values in the ROIs were measured using a Bio-Imaging Analyzer System (BAS5000, FUJIFILM).

PET Assessment. A rat was secured in a custom-designed chamber and placed in a small animal PET scanner (Inveon, Siemens Medical Solutions, Knoxville, TN). Body temperature was maintained using a 40 °C water circulation system (T/Pump TP401, Gaymar Industries, Orchard Park, NY). A 24 G intravenous catheter (Terumo Medical Products, Tokyo, Japan) was placed in the tail vein of the rat for a bolus injection. A bolus of [^{11}C]**10** (1 mL, 37–49 MBq, 0.1–0.7 nmol) was injected at flow rate of 0.5 mL/min via the catheter inserted into the tail vein. For blocking experiments, compound **1** (n = 4, 1 mg/kg) was administrated prior to a bolus injection of [^{11}C]**10**. Dynamic emission scans in three-dimensional list mode were performed for 60 min (10 s × 12 frames, 20 s × three frames, 30 s × three frames, 60 s × three frames, 150 s × three frames, and 300 s × nine frames). Acquired PET dynamic images were reconstructed by filtered back projection using

Hanning's filter with a Nyquist cutoff of 0.5 cycle/pixel, which were summed using analysis software (ASIPro VM™, Siemens Medical Solutions). The TACs of [^{11}C]**10** were acquired from volumes of interest in the frontal cortex, striatum (caudate/putamen), hippocampus, thalamus, and cerebellum referring to a rat brain MRI template[42] using PMOD software (version 3.4; PMOD technology, Zurich, Switzerland). The radioactivity was decay-corrected to the injection time and is expressed as the standardized uptake value (SUV) that was normalized to the injected radioactivity and body weight. SUVs were calculated according to the following formula: SUV = (radioactivity per milliliter tissue per injected radioactivity) × gram of body weight. To obtain BP_{ND}, kinetic analysis with SRTM was performed using PMOD software. A reference region for mGluR5 was chosen in the cerebellum.[40] Representative parametric images scaled with BP_{ND} were reconstructed by PMOD software using TACs in mGluR5-enriched and reference regions. For test-retest PET studies, seven male SD rats were used twice within 7–10 days (247 ± 45 g at first and 303 ± 44 g at the second scan), and the reliability of the data was assessed by the ICC. The parameters were calculated as follows:

a. Relative difference (%) = (scan 2 – scan 1)/scan 1 × 100

b. Test-retest variability (%) = |scan 2 – scan 1|/[(scan 2 + scan 1)/2] × 100

c. Coefficient of variation (%CV) = standard deviation (s.d.)/mean × 100

d. ICC with BSMSS as "mean sum of squares between subjects" and WSMSS as "mean sum of squares within subjects": ICC = (BSMSS – WSMSS)/(BSMSS + WSMSS). An ICC value of −1

denotes no reliability, whereas 1 indicates maximum reliability.[39]

Ex Vivo Metabolite Analysis. Following intravenous injection of [^{11}C]**10** (60–108 MBq, 0.2–0.4 mL, 1–2 nmol), the rats (n = 3 for each time point) were sacrificed by cervical dislocation at 5, 30, and 60 min. Blood and whole brain samples were obtained quickly. The blood sample was centrifuged at 15,000 g for 2 min at 4 °C to separate the plasma. The supernatant (0.5 mL) was collected in a test tube containing MeCN (0.5 mL), and the resulting mixture was vortexed for 15 s and then centrifuged at 15,000 g for 2 min for deproteinization. The resulting supernatant was collected. The rat brain was homogenized with a Silent Crusher S homogenizer in an ice-cooled MeCN/H_2O (1/1, 2 mL) solution. The resulting homogenate was centrifuged at 15,000 g for 2 min at 4 °C. The supernatant (0.5 mL) was collected, resuspended with MeCN (0.5 mL), and then centrifuged at 15,000 g for 2 min for deproteinization. An aliquot of the supernatant (0.1–1.0 mL) obtained from the plasma or brain homogenate was injected into the HPLC system with a radioactivity detector[42] and analyzed using a Capcell Pak C_{18} column (4.6 mm i.d. × 250 mm) with a mobile phase (MeCN/H_2O/Et_3N, (55/45/0.01, v/v/v)) at a flow rate of 1.5 mL/min. The percentage ratio of [^{11}C]**10** (t_R = 5.1–5.4 min) to total radioactivity (corrected for decay) on the HPLC chromatogram was calculated as % = (peak area for [^{11}C]ligand/total peak area) × 100.

Biodistribution Analysis. Each mouse (34–38 g) was injected a bolus of [^{11}C]**10** (4.8 MBq/0.1 mL,

40 pmol) via the tail vein. Three mice were sacrificed at each experimental time point (1, 5, 15, 30, and 60 min) after injection by cervical dislocation. The whole brain, heart, liver, lung, spleen, testis, kidney, pancreas, stomach (including contents), small intestines (including contents), large intestines (including contents), muscle, and blood samples were removed quickly. The radioactivity in these tissues was measured with an autogamma scintillation counter (1480 Wizard) and expressed as the %ID/g. All radioactivity measurements were corrected for decay.

Statistics

All data are expressed as means ± s.d. The relationship between the regional outcome parameters under test and retest conditions were estimated using GraphPad Prism 5 software.

ASSOCIATED CONTENT

Supporting Information

Purities of compounds **9–15** determined by HPLC; HPLC analytical charts for **9–15**; HPLC purification charts for [^{11}C]**9** and [^{11}C]**10**; Time course for the ratio of radioactivities in ROIs against the cerebellum; Radio-HPLC charts for metabolite analysis in the plasma and brains of rats.

AUTHOR INFORMATION

Corresponding Author

*Phone: +81-43-382-3709; Fax: +81-43-206-3261; E-mail: zhang@nirs.go.jp.

Author Contributions

§Y.S., T.Y., and M.F. contributed equally.

Notes

The authors declare no competing financial interest.

ACKNOWLEDGMENTS

We would like to thank the staff at the National Institute of Radiological Sciences for their support with the cyclotron operation, radioisotope production, radiosynthesis, and animal experiments.

ABBREVIATIONS USED

BP_{ND}, nondisplaceable binding potential; EOB, end of bombardment; EOS, end of synthesis; ICC, intra class correlation coefficient; mGluR1, metabotropic glutamate receptor type 1; mGluR5, metabotropic glutamate receptor type 5; %ID/g, percentage of the injected dose per gram of wet tissue; *r*, Pearson's correlation coefficient; ROI, region of interest; SRTM, simplified reference tissue model; SUV, standardized uptake value; TAC, time-activity curve.

REFERENCES

(1) Ferraguti, F.; Crepaldi, L.; Nicoletti, F. Metabotropic glutamate 1 receptor: current concepts and perspectives. *Pharmacol. Rev.* **2008**, *60*, 536–581.

(2) Hermans, E.; Challiss, R. A. Structural, signalling and regulatory properties of the group I metabotropic glutamate receptors: prototypic family C G-protein-coupled receptors. *Biochem. J.* **2001**, *359*, 465–484.

(3) Aramori, I.; Nakanishi, S. Signal transduction and pharmacological characteristics of a metabotropic glutamate receptor, mGluR1, in transfected CHO cells. *Neuron* **1992**, *8*, 757–765.

(4) Francesconi, A.; Duvoisin, R. M. Role of the second and third intracellular loops of metabotropic glutamate receptors in mediating dual signal transduction activation. *J. Biol. Chem.* **1998**, *273*, 5615–5624.

(5) Abe, T.; Sugihara, H.; Nawa, H.; Shigemoto, R.; Mizuno, N.; Nakanishi, S. Molecular characterization of a novel metabotropic glutamate receptor mGluR5 coupled to inositol phosphate/Ca^{2+} signal transduction. *J. Biol. Chem.* **1992**, *267*, 13361–13368.

(6) Fotuhi, M.; Sharp, A. H.; Glatt, C. E.; Hwang, P. M.; von Krosigk, M.; Snyder, S. H.; Dawson, T. M. Differential localization of phosphoinositide-linked metabotropic glutamate receptor (mGluR1) and the inositol 1,4,5-trisphosphate receptor in rat brain. *J. Neurosci.* **1993**, *13*, 2001–2012.

(7) Alagarsamy, S.; Marino, M. J.; Rouse, S. T.; Gereau, R. W. t.; Heinemann, S. F.; Conn, P. J.

Activation of NMDA receptors reverses desensitization of mGluR5 in native and recombinant systems. *Nat. Neurosci.* **1999**, *2*, 234–240.

(8) Page, G.; Peeters, M.; Najimi, M.; Maloteaux, J. M.; Hermans, E. Modulation of the neuronal dopamine transporter activity by the metabotropic glutamate receptor mGluR5 in rat striatal synaptosomes through phosphorylation mediated processes. *J. Neurochem.* **2001**, *76*, 1282–1290.

(9) Salt, T. E.; Binns, K. E.; Turner, J. P.; Gasparini, F.; Kuhn, R. Antagonism of the mGlu5 agonist 2-chloro-5-hydroxyphenylglycine by the novel selective mGlu5 antagonist 6-methyl-2-(phenylethynyl)-pyridine (MPEP) in the thalamus. *Br. J. Pharmacol.* **1999**, *127*, 1057–1259.

(10) Walles, M.; Wolf, T.; Jin, Y.; Ritzau, M.; Leuthold, L. A.; Krauser, J.; Gschwind, H. P.; Carcache, D.; Kittelmann, M.; Ocwieja, M.; Ufer, M.; Woessner, R.; Chakraborty, A.; Swart, P. Metabolism and disposition of the metabotropic glutamate receptor 5 antagonist (mGluR5) mavoglurant (AFQ056) in healthy subjects. *Drug Metab. Dispos.* **2013**, *41*, 1626–1641.

(11) Swedberg, M. D.; Raboisson, P. AZD9272 and AZD2066: Selective and highly central nervous system penetrant mGluR5 antagonists characterized by their discriminative effects. *J. Pharmacol. Exp. Ther.* **2014**, *350*, 212–222.

(12) Gasparini, F.; Lingenhohl, K.; Stoehr, N.; Flor, P. J.; Heinrich, M.; Vranesic, I.; Biollaz, M.; Allgeier, H.; Heckendorn, R.; Urwyler, S.; Varney, M. A.; Johnson, E. C.; Hess, S. D.; Rao, S. P.; Sacaan, A. I.; Santori, E. M.; Velicelebi, G.; Kuhn, R. 2-Methyl-6-(phenylethynyl)-pyridine (MPEP),

a potent, selective and systemically active mGlu5 receptor antagonist. *Neuropharmacology* **1999**, *38*, 1493–1503.

(13) Cosford, N. D.; Tehrani, L.; Roppe, J.; Schweiger, E.; Smith, N. D.; Anderson, J.; Bristow, L.; Brodkin, J.; Jiang, X.; McDonald, I.; Rao, S.; Washburn, M.; Varney, M. A. 3-[(2-Methyl-1,3-thiazol-4-yl)ethynyl]-pyridine: a potent and highly selective metabotropic glutamate subtype 5 receptor antagonist with anxiolytic activity. *J. Med. Chem.* **2003**, *46*, 204–206.

(14) Yu, M. Recent developments of the PET imaging agents for metabotropic glutamate receptor subtype 5. *Curr. Top. Med. Chem.* **2007**, *7*, 1800–1805.

(15) Mu, L.; Schubiger, P. A.; Ametamey, S. M. Radioligands for the PET imaging of metabotropic glutamate receptor subtype 5 (mGluR5). *Curr. Top. Med. Chem.* **2010**, *10*, 1558–1568.

(16) Ametamey, S. M.; Treyer, V.; Streffer, J.; Wyss, M. T.; Schmidt, M.; Blagoev, M.; Hintermann, S.; Auberson, Y.; Gasparini, F.; Fischer, U. C.; Buck, A. Human PET studies of metabotropic glutamate receptor subtype 5 with ^{11}C-ABP688. *J. Nucl. Med.* **2007**, *48*, 247–252.

(17) Kimura, Y.; Simeon, F. G.; Hatazawa, J.; Mozley, P. D.; Pike, V. W.; Innis, R. B.; Fujita, M. Biodistribution and radiation dosimetry of a positron emission tomographic ligand, ^{18}F-SP203, to image metabotropic glutamate subtype 5 receptors in humans. *Eur. J. Nucl. Med. Mol. Imaging* **2010**, *37*, 1943–1949.

(18) Sullivan, J. M.; Lim, K.; Labaree, D.; Lin, S. F.; McCarthy, T. J.; Seibyl, J. P.; Tamagnan, G.; Huang, Y.; Carson, R. E.; Ding, Y. S.; Morris, E. D. Kinetic analysis of the metabotropic glutamate

subtype 5 tracer [^{18}F]FPEB in bolus and bolus-plus-constant-infusion studies in humans. *J. Cereb. Blood Flow Metab.* **2013**, *33*, 532–541.

(19) Kågedal, M.; Cselényi, Z.; Nyberg, S.; Jönsson, S.; Raboisson, P.; Stenkrona, P.; Hooker, A.C.; Karlsson, M.O. Non-liner mized effects modelling of positron emission tomography data for simultaneous estimation of radioligand kinetics and occupancy in healthy vulunteers. *NeuroImage* **2012**, *61*, 849–856.

(20) Milella, M. S.; Marengo, L.; Larcher, K.; Fotros, A.; Dagher, A.; Rosa-Neto, P.; Benkelfat, C.; Leyton, M. Limbic system mGluR5 availability in cocaine dependent subjects: a high-resolution PET [^{11}C]ABP688 study. *NeuroImage* **2014**, *98*, 195–202.

(21) Kagedal, M.; Cselenyi, Z.; Nyberg, S.; Raboisson, P.; Stahle, L.; Stenkrona, P.; Varnas, K.; Halldin, C.; Hooker, A. C.; Karlsson, M. O. A positron emission tomography study in healthy volunteers to estimate mGluR5 receptor occupancy of AZD2066 — estimating occupancy in the absence of a reference region. *NeuroImage* **2013**, *82*, 160–169.

(22) Deschwanden, A.; Karolewicz, B.; Feyissa, A. M.; Treyer, V.; Ametamey, S. M.; Johayem, A.; Burger, C.; Auberson, Y. P.; Sovago, J.; Stockmeier, C. A.; Buck, A.; Hasler, G. Reduced metabotropic glutamate receptor 5 density in major depression determined by [^{11}C]ABP688 PET and postmortem study. *Am. J. Psychiatry* **2011**, *168*, 727–734.

(23) Ametamey, S. M.; Kessler, L. J.; Honer, M.; Wyss, M. T.; Buck, A.; Hintermann, S.; Auberson, Y. P.; Gasparini, F.; Schubiger, P. A. Radiosynthesis and preclinical evaluation of

^{11}C-ABP688 as a probe for imaging the metabotropic glutamate receptor subtype 5. *J. Nucl. Med.* **2006**, *47*, 698–705.

(24) Li, P. X.; Olszewski, J. D. Radiosynthesis of [^{3}H]-ABP688 using [^{3}H]-methyl nosylate: a non-volatile alternative methylating agent. *J. Labelled Comp. Radiopharm.* **2009**, *52*, 512–513.

(25) Kawamura, K.; Yamasaki, T.; Kumata, K.; Furutsuka, K.; Takei, M.; Wakizaka, H.; Fujinaga, M.; Kariya, K.; Yui, J.; Hatori, A.; Xie, L.; Shimoda, Y.; Hashimoto, H.; Hayashi, K.; Zhang, M. R. Binding potential of (*E*)-[^{11}C]ABP688 to metabotropic glutamate receptor subtype 5 is decreased by the inclusion of its ^{11}C-labelled *Z*-isomer. *Nucl. Med. Biol.* **2014**, *41*, 17–23.

(26) DeLorenzo, C.; Kumar, J. S.; Mann, J. J.; Parsey, R. V. In vivo variation in metabotropic glutamate receptor subtype 5 binding using positron emission tomography and [^{11}C]ABP688. *J. Cereb. Blood Flow Metab.* **2011**, *31*, 2169–2180.

(27) DeLorenzo, C.; Milak, M. S.; Brennan, K. G.; Kumar, J. S.; Mann, J. J.; Parsey, R. V. In vivo positron emission tomography imaging with [^{11}C]ABP688: binding variability and specificity for the metabotropic glutamate receptor subtype 5 in baboons. *Eur. J. Nucl. Med. Mol. Imaging* **2011**, *38*, 1083–1094.

(28) Park, E.; Sullivan, J. M.; Planeta, B.; Gallezot, J. D.; Lim, K.; Lin, S. F.; Ropchan, J.; McCarthy, T. J.; Ding, Y. S.; Morris, E. D.; Williams, W. A.; Huang, Y.; Carson, R. E. Test-retest reproducibility of the metabotropic glutamate receptor 5 ligand [^{18}F]FPEB with bolus plus constant infusion in humans. *Eur. J. Nucl. Med. Mol. Imaging* **2015**, *42*, 1530–1541.

(29) Sephton, S. M.; Herde, A. M.; Mu, L.; Keller, C.; Rudisuhli, S.; Auberson, Y.; Schibli, R.; Kramer, S. D.; Ametamey, S. M. Preclinical evaluation and test-retest studies of [^{18}F]PSS232, a novel radioligand for targeting metabotropic glutamate receptor 5 ($mGlu_5$). *Eur. J. Nucl. Med. Mol. Imaging* **2015**, *42*, 128–137.

(30) Zhuo, X.; Huang, X. S.; Degnan, A. P.; Snyder, L. B.; Yang, F.; Huang, H.; Shu, Y. Z.; Johnson, B. M. Identification of glutathione conjugates of acetylene-containing positive allosteric modulators of metabotropic glutamate receptor subtype 5. *Drug Metab. Dispos.* **2015**, *43*, 578–589.

(31) Tehrani, L. R.; Smith, N. D.; Huang, D.; Poon, S. F.; Roppe, J. R.; Seiders, T. J.; Chapman, D. F.; Chung, J.; Cramer, M.; Cosford, N. D. 3-[Substituted]-5-(5-pyridin-2-yl-2*H*-tetrazol-2-yl)benzonitriles: identification of highly potent and selective metabotropic glutamate subtype 5 receptor antagonists. *Bioorg. Med. Chem. Lett.* **2005**, *15*, 5061–5064.

(32) Roppe, J.; Smith, N. D.; Huang, D.; Tehrani, L.; Wang, B.; Anderson, J.; Brodkin, J.; Chung, J.; Jiang, X.; King, C.; Munoz, B.; Varney, M. A.; Prasit, P.; Cosford, N. D. Discovery of novel heteroarylazoles that are metabotropic glutamate subtype 5 receptor antagonists with anxiolytic activity. *J. Med. Chem.* **2004**, *47*, 4645–4648.

(33) Pike, V. W. PET radiotracers: crossing the blood-brain barrier and surviving metabolism. *Trends Pharmacol. Sci.* **2009**, *30*, 431–440.

(34) Shigemoto, R.; Nomura, S.; Ohishi, H.; Sugihara, H.; Nakanishi, S.; Mizuno, N.

Immunohistochemical localization of a metabotropic glutamate receptor, mGluR5, in the rat brain. *Neurosci. Lett.* **1993**, *163*, 53–57.

(35) Lavreysen, H.; Wouters, R.; Bischoff, F.; Nobrega Pereira, S.; Langlois, X.; Blokland, S.; Somers, M.; Dillen, L.; Lesage, A. S. JNJ16259685, a highly potent, selective and systemically active mGlu1 receptor antagonist. *Neuropharmacology* **2004**, *47*, 961–972.

(36) Lammertsma, A. A.; Hume, S. P. Simplified reference tissue model for PET receptor studies. *NeuroImage* **1996**, *4*, 153–158.

(37) Mintun, M. A.; Raichle, M. E.; Kilbourn, M. R.; Wooten, G. F.; Welch, M. J. A quantitative model for the in vivo assessment of drug binding sites with positron emission tomography. *Ann. Neurol.* **1984**, *15*, 217–227.

(38) Yamasaki, T.; Fujinaga, M.; Kawamura, K.; Yui, J.; Hatori, A.; Ohya, T.; Xie, L.; Wakizaka, H.; Yoshida, Y.; Fukumura, T.; Zhang, M. R. In vivo measurement of the affinity and density of metabotropic glutamate receptor subtype 1 in rat brain using ^{18}F-FITM in small-animal PET. *J. Nucl. Med.* **2012**, *53*, 1601–1607.

(39) Elmenhorst, D.; Aliaga, A.; Bauer, A.; Rosa-Neto, P. Test-retest stability of cerebral $mGluR_5$ quantification using [^{11}C]ABP688 and positron emission tomography in rats. *Synapse* **2012**, *66*, 552–560.

(40) Elmenhorst, D.; Minuzzi, L.; Aliaga, A.; Rowley, J.; Massarweh, G.; Diksic, M.; Bauer, A.; Rosa-Neto, P. In vivo and in vitro validation of reference tissue models for the $mGluR_5$ ligand

[^{11}C]ABP688. *J. Cereb. Blood Flow Metab.* **2010**, *30*, 1538–1549.

(41) Zhang, M.-R.; Kida, T.; Noguchi, J.; Furutsuka, K.; Maeda, J.; Suhara, T.; Suzuki, K. [^{11}C]DAA1106: radiosynthesis and in vivo binding to peripheral benzodiazepine receptors in mouse brain. *Nucl. Med. Biol*. **2003**, *30*, 513–519.

(42) Yui, J.; Hatori, A.; Kawamura, K.; Yanamoto, K.; Yamasaki, T.; Ogawa, M.; Yoshida, Y.; Kumata, K.; Fujinaga, M.; Nengaki, N.; Fukumura, T.; Suzuki, K.; Zhang, M. R. Visualization of early infarction in rat brain after ischemia using a translocator protein (18 kDa) PET ligand [^{11}C]DAC with ultra-high specific activity. *NeuroImage* **2011**, *54*, 123–130.

(43) Takei, M.; Kida, T.; Suzuki, K. Sensitive measurement of positron emitters eluted from HPLC. *Appl. Radiat. Isot.* **2001**, *55*, 229–234.

Table 1. In vitro-binding affinity and lipophilicity of PET ligand candidates **9**–**13**

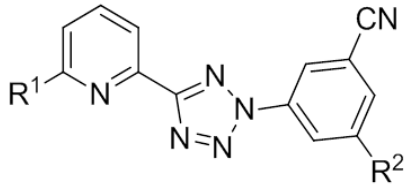

Compd	R^1	R^2	Affinity for mGluR5		Lipophilicity	
			IC_{50} (nM)	K_i (nM)	cLogD[a]	LogD
9	H	OCH_3	13.7 ± 6.3	10.8 ± 5.2	2.7	2.4
11	F	OCH_3	566 ± 248	438 ± 190	2.9	n/a
12	CH_3	OCH_3	2915 ± 2767	2280 ± 2155	2.9	n/a
10	H	CH_3	11.9 ± 5.8	9.4 ± 4.7	2.4	2.8
13	H	OCH_2CH_2F	141 ± 52	108 ± 38	2.4	n/a
3	—	—	6.9 ± 2.6	5.5 ± 2.3	3.3	2.4[b]

[a]cLogD values were calculated with ADMET Predictor™. [b]Value was obtained from reference 14.

Table 2. Ratios (means ± s.d.) of brain regions to the cerebellum in autoradiographic studies with [^{11}C]**9** and [^{11}C]**10**

Region	[^{11}C]**9**			[^{11}C]**10**		
	Control	+ **1** (1 μM)	+ **25** (1 μM)	Control	+ **1** (1 μM)	+ **25** (1 μM)
Striatum	14.9 ± 1.8	2.7 ± 0.6	13.5 ± 1.2	15.8 ± 0.8	2.1 ± 0.9	15.3 ± 0.5
Hippocumpus	13.6 ± 2.8	2.4 ± 0.8	12.3 ± 1.6	13.6 ± 1.0	1.6 ± 0.4	12.1 ± 0.7
Cerebral cortex	12.2 ± 1.3	1.9 ± 0.4	10.9 ± 1.2	9.9 ± 0.7	1.2 ± 0.3	9.5 ± 0.5
Thalamus	8.8 ± 4.5	2.4 ± 0.7	7.5 ± 3.3	4.4 ± 0.4	1.9 ± 0.6	4.3 ± 0.2
Meddula/Pons	3.2 ± 0.4	3.5 ± 1.2	3.7 ± 0.2	2.6 ± 0.4	1.5 ± 0.5	2.4 ± 0.2

Table 3. Reliability of outcome parameters in test-retest PET studies with [^{11}C]**10**

	BP_{ND} Test		BP_{ND} Retest		% rel Diff.		% Variability			
Region	Mean	± s.d.	Mean	± s.d.	Mean	± s.d.	Mean	± s.d.	ICC	*r*
Striatum	1.30	± 0.10	1.30	± 0.12	−0.2	± 3.7	3.0	± 1.7	0.90	0.91
Hippocampus	0.94	± 0.09	1.00	± 0.13	6.1	± 5.1	5.9	± 4.7	0.78	0.95
Frontal cortex	0.82	± 0.09	0.87	± 0.12	4.9	± 8.6	7.3	± 5.3	0.74	0.80
Thalamus	0.72	± 0.09	0.70	± 0.09	−2.4	± 8.9	8.5	± 2.7	0.73	0.72

Abbreviations: rel Diff, relative difference; ICC, intraclass correlation coefficient; *r*, correlation coefficient.

Scheme 1. Synthesis of **9–16**[a]

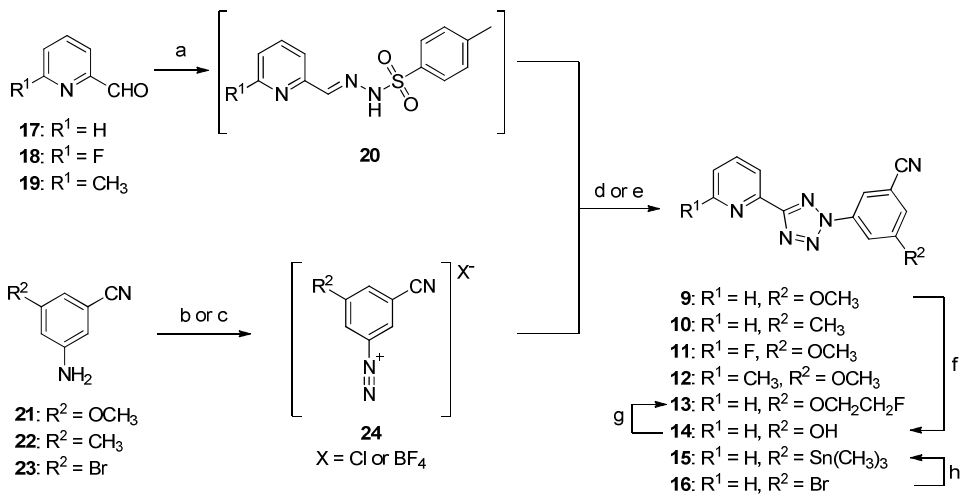

[a] Reagents and conditions: (a) *p*-toluenesulfonyl hydrazide, EtOH or CH_2Cl_2, room temperature, 15–60 min; (b) EtOH, H_2O, HBF_4, then $NaNO_2$, −5 °C; (c) EtOH, H_2O, HCl, then $NaNO_2$, −5 °C; (d) pyridine, −10 °C to room temperature, 2–3.5 h; (e) NaOH, H_2O, −10 °C, 3.5 h; (f) 1 M BBr_3, CH_2Cl_2, −40 °C to room temperature, overnight; (g) 2-fluoroethyl 4-methylbenzenesulfonate, K_2CO_3, DMF, 70 °C, 5 h; (h) hexamethylditin, $Pd(PPh_3)_4$, 1,4-dioxane, 110 °C, 16 h.

Scheme 2. Radiosynthesis of [^{11}C]**9** and [^{11}C]**10**

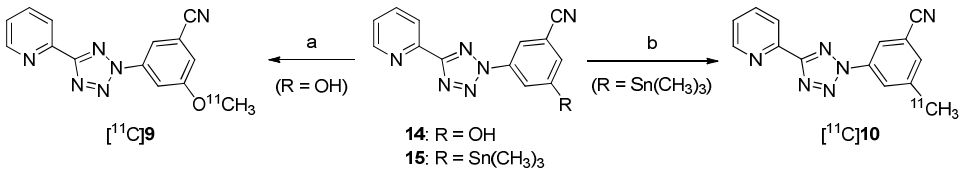

[^{11}C]**9** **14**: R = OH **15**: R = Sn(CH$_3$)$_3$ [^{11}C]**10**

[a] Reagents and conditions: (a) [^{11}C]MeI, NaOH, DMF, 70 °C, 5 min; (b) [^{11}C]MeI, $Pd_2(dba)_3$, P(*o*-tol)$_3$, CuCl, CsF, DMF, 80 °C, 5 min.

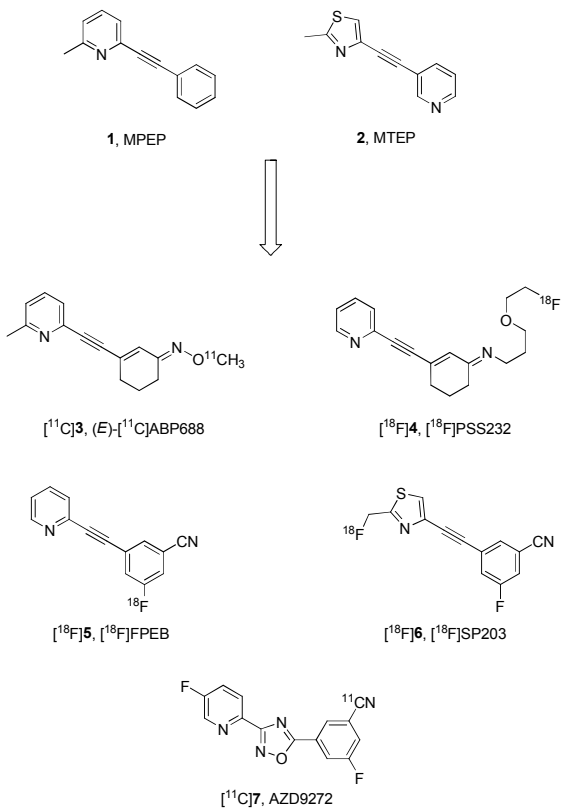

Figure 1. Two primary modulators of mGluR5 and their radiolabeled derivatives for clinical PET studies.

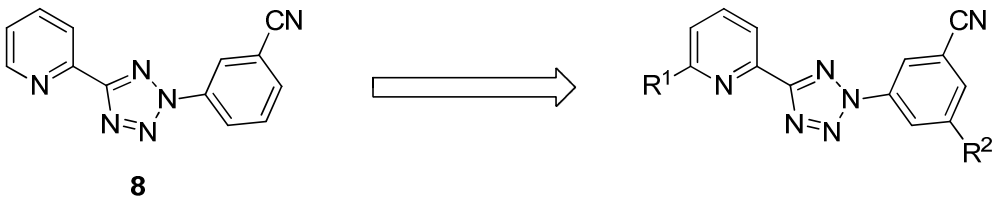

9: R^1 = H, R^2 = OCH_3
10: R^1 = H, R^2 = CH_3
[^{11}C]**9**: R^1 = H, R^2 = $O^{11}CH_3$
[^{11}C]**10**: R^1 = H, R^2 = $^{11}CH_3$
11: R^1 = F, R^2 = OCH_3
12: R^1 = CH_3, R^2 = OCH_3
13: R^1 = H, R^2 = OCH_2CH_2F
14: R^1 = H, R^2 = OH
15: R^1 = H, R^2 = $Sn(CH_3)_3$

Figure 2. Chemical structures of **9**–**15** and their radiolabeled compounds [^{11}C]**9** and [^{11}C]**10**.

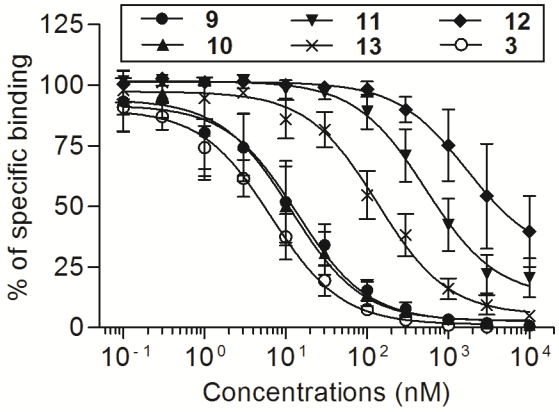

Figure 3. In vitro binding assay of compounds **3**, **9**–**13** using rat brain homogenates with [^{11}C]**3**. Compounds **3** and **9**–**13** were analyzed at various concentrations (10^{-1}–10^{4} nM). Percentages (n = 3, means ± s.d.) of specific binding indicated inhibition of test compounds against mGluR5 with [^{11}C]**3**. All curves were obtained by least square fitting.

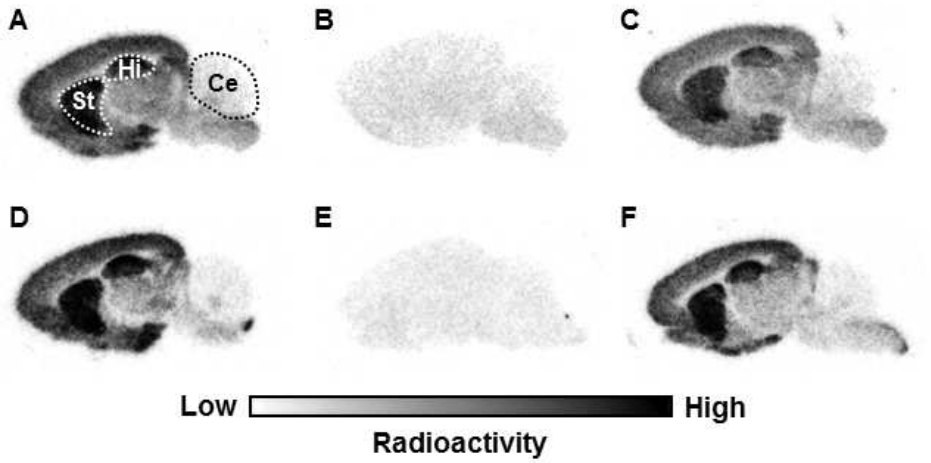

Figure 4. Representative in vitro autoradiograms of [^{11}C]**9** (A–C) and [^{11}C]**10** (D–F) using rat brain sections. Brain sections (n = 3) were treated with the vehicle (A and D), 1 μM **1** (B and E), or 1 μM **25** (C and F). Ce: cerebellum, Hi: hippocampus, St: striatum.

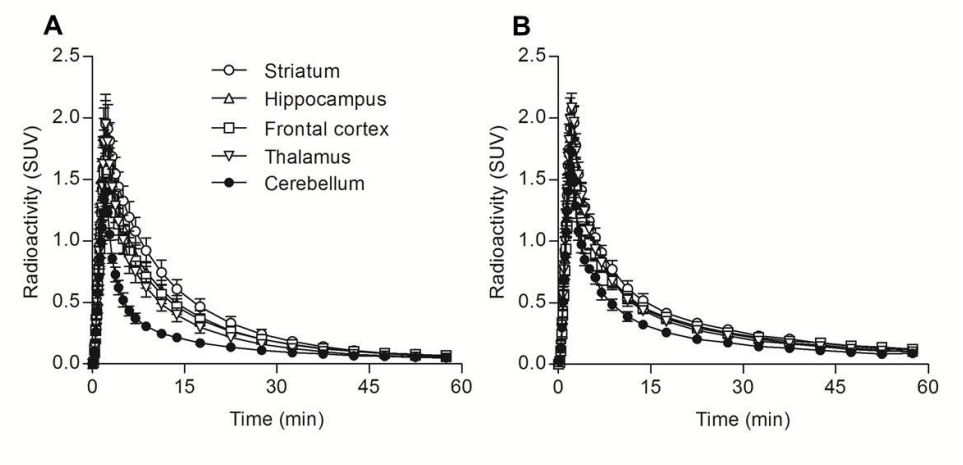

Figure 5. TACs of [^{11}C]**10** (means ± s.d.). A rat was treated with [^{11}C]**10** in saline (A, n = 7) or 1 mg/kg compound **1** (B, n = 4). ROIs were located on the striatum (open circles), hippocampus (open upper triangles), frontal cortex (open squares), thalamus (open lower triangles), and cerebellum (buried circles). Radioactivity is expressed as SUVs.

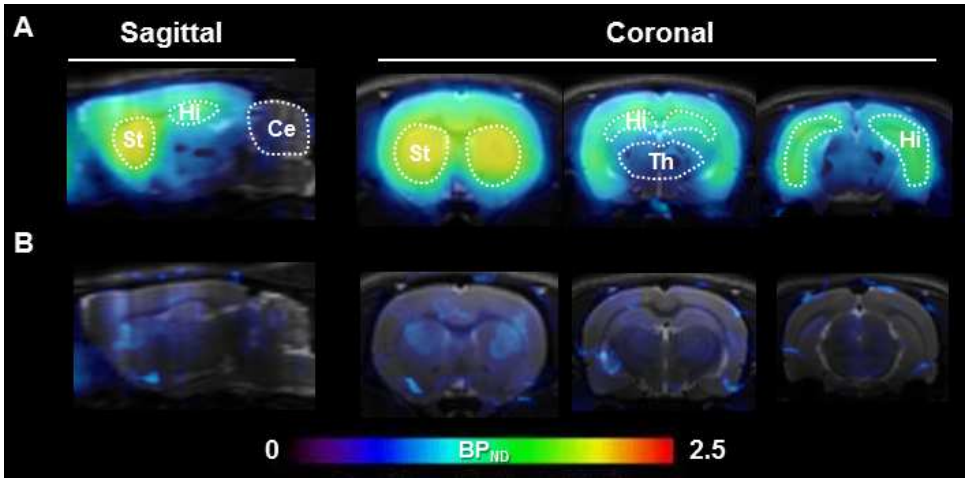

Figure 6. Representative parametric PET/MRI images of [^{11}C]**10** in rat brain. A: baseline, B: 1 mg/kg compound **1**. Signals were scaled with BP_{ND} values based on SRTM.

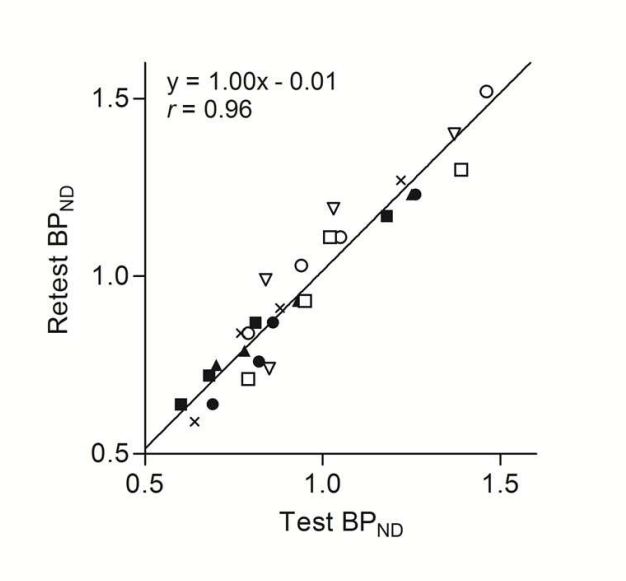

Figure 7. Correlation between test and retest BP_{ND} values in PET studies with [^{11}C]**10** (n = 7 and 4 regions each).

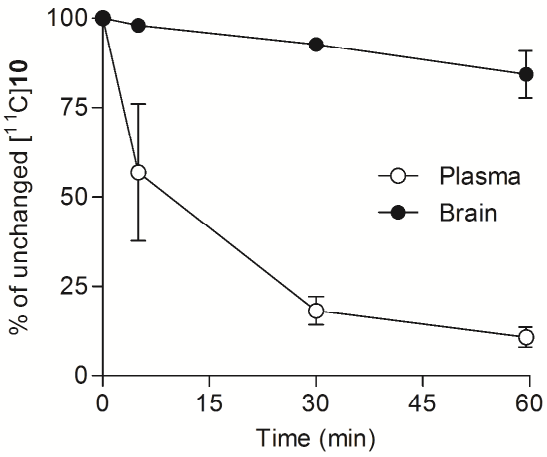

Figure 8. Time course of percentages (means ± s.d.) of unchanged [^{11}C]**10** in the plasma and brains of rats (n = 3).

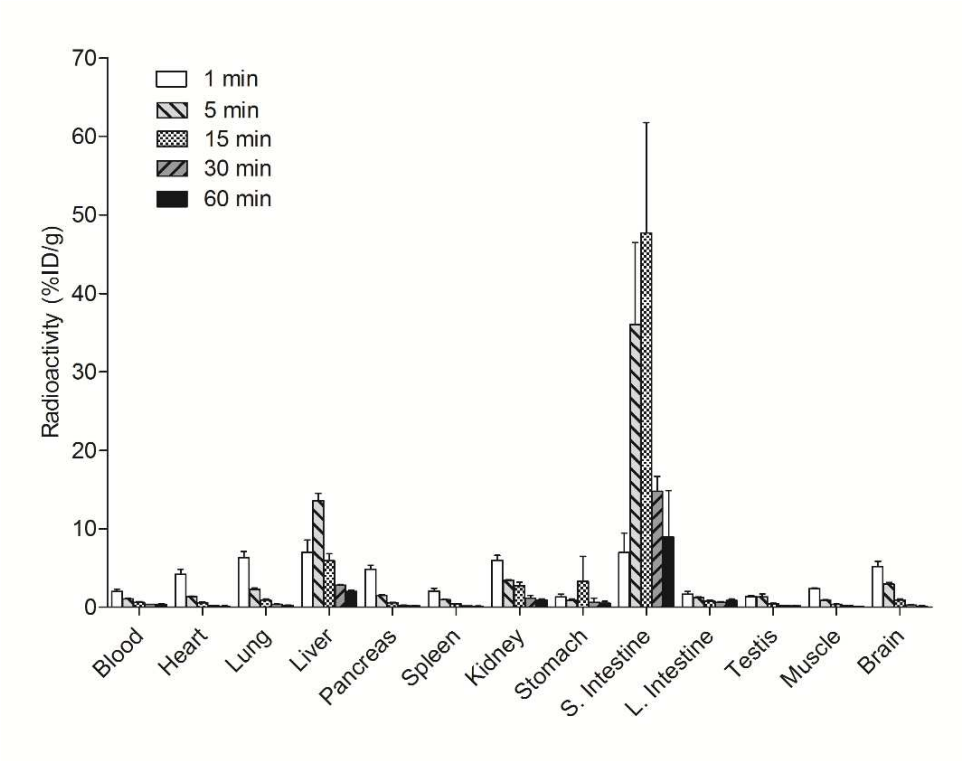

Figure 9. Biodistribution (means ± s.d.) of [^{11}C]**10** in the whole body of mice. Mice (n = 3) were sacrificed at 1, 5, 15, 30, and 60 min after injection of [^{11}C]**10**.

Table of Contents graphic